NEUROSCIENCE

Glucose-sensing glucagon-like peptide-1 receptor neurons in the dorsomedial hypothalamus regulate glucose metabolism

Zhaohuan Huang[1,2]†, Ling Liu[1,2]†, Jian Zhang[3]†, Kristie Conde[4,5], Jay Phansalkar[4,5], Zhongzhong Li[1], Lei Yao[3], Zihui Xu[4,5], Wei Wang[6], Jiangning Zhou[3], Guoqiang Bi[2,3], Feng Wu[1,2], Randy J. Seeley[7], Michael M. Scott[8], Cheng Zhan[9,10,11], Zhiping P. Pang[4,5], Ji Liu[1,2,3]*

Glucagon-like peptide-1 (GLP-1) regulates energy homeostasis via activation of the GLP-1 receptors (GLP-1Rs) in the central nervous system. However, the mechanism by which the central GLP-1 signal controls blood glucose levels, especially in different nutrient states, remains unclear. Here, we defined a population of glucose-sensing GLP-1R neurons in the dorsomedial hypothalamic nucleus (DMH), by which endogenous GLP-1 decreases glucose levels via the cross-talk between the hypothalamus and pancreas. Specifically, we illustrated the sufficiency and necessity of DMH$^{GLP\text{-}1R}$ in glucose regulation. The activation of the DMH$^{GLP\text{-}1R}$ neurons is mediated by a cAMP-PKA–dependent inhibition of a delayed rectifier potassium current. We also dissected a descending control of DMH$^{GLP\text{-}1R}$ –dorsal motor nucleus of the vagus nerve (DMV)–pancreas activity that can regulate glucose levels by increasing insulin release. Thus, our results illustrate how central GLP-1 action in the DMH can induce a nutrient state–dependent reduction in blood glucose level.

INTRODUCTION

Glucagon-like peptide-1 (GLP-1), a gut-brain hormone, is a post-translational cleavage product of preproglucagon encoded by the *Gcg* gene (*1*–*5*). In the periphery, GLP-1 is secreted postprandially from the gut and augments insulin release depending on the availability of glucose (*3*, *4*, *6*–*9*). In the central nervous system, GLP-1 is mainly produced by a subpopulation of neurons in the nucleus tractus solitarius (NTS) (*10*, *11*). GLP-1 neurons send robust projections to various forebrain regions, especially to the feeding control centers of the paraventricular nucleus of hypothalamus (PVN) and the dorsomedial hypothalamic nucleus (DMH) (*12*, *13*). The roles of hypothalamic GLP-1 in the regulation of feeding behavior have been intensively investigated, yet the function of central GLP-1 in the regulation of glucose metabolism remains controversial. While most studies reported a hypoglycemic effect (*11*, *14*), others have observed a hyperglycemic effect after central GLP-1 treatment (*15*). Thus, it is important to understand whether and how central GLP-1 affects glucose metabolism.

[1]National Engineering Laboratory for Brain-inspired Intelligence Technology and Application, School of Information Science and Technology, University of Science and Technology of China, Anhui, China. [2]Institute of Artificial Intelligence, Hefei Comprehensive National Science Center, Hefei, China. [3]CAS Key Laboratory of Brain Function and Diseases, Life Science School, University of Science and Technology of China, Anhui, China. [4]Child Health Institute of New Jersey, Rutgers University Robert Wood Johnson Medical School, New Brunswick, NJ 08901, USA. [5]Department of Neuroscience and Cell Biology, Rutgers University Robert Wood Johnson Medical School, New Brunswick, NJ 08901, USA. [6]Department of Endocrinology and Laboratory for Diabetes, The First Affiliated Hospital of USTC, Division of Life Sciences and Medicine, University of Science and Technology of China, Anhui, China, [7]Department of Surgery, University of Michigan, Ann Arbor, MI 48109, USA. [8]Department of Pharmacology, University of Virginia, Charlottesville, VA 22908, USA. [9]Department of Hematology, The First Affiliated Hospital, Life Science School, University of Science and Technology of China, Anhui, China. [10]National Institute of Biological Sciences, Beijing 102206, China. [11]Tsinghua Institute of Multidisciplinary Biomedical Research, Tsinghua University, Beijing 100084, China.
*Corresponding author. Email: geeliu6@gmail.com
†These authors contributed equally to this work.

GLP-1 receptor (GLP-1R) is a G protein (heterotrimeric GTP-binding protein)–coupled receptor that is expressed abundantly in both the periphery (*16*) and the brain, including the PVN, DMH, and the arcuate nucleus (ARC) (*12*). Previously, we reported an intracellular signaling pathway responsible for regulating feeding behavior in the PVN, involving phosphorylation of glutamatergic AMPA receptor subunit GluA1, followed by enhanced AMPA receptor membrane trafficking postsynaptic excitation (*17*). However, it is not clear whether the same intracellular signaling pathway or a different one regulates glucose metabolism.

One important advantage of GLP-1–based therapies for diabetes is that GLP-1–induced insulin release is dependent on circulating glucose levels, making GLP-1–based therapies less likely than other insulin secretagogues to cause hypoglycemia (*3*, *4*). GLP-1 signaling in the brain with regard to feeding behavior and glucose metabolism is also likely to be affected by the nutritional status of the animal (*8*, *18*, *19*), a hypothesis that has yet to be fully investigated.

To address these outstanding questions, we investigated the neural basis of how central GLP-1 regulates glucose levels. We also addressed the possible intracellular signaling pathway induced by activation of GLP-1R in doing so. Last, we investigated how integrating the GLP-1 signal and nutrient state in the hypothalamus affects glucose levels.

RESULTS

Exogenous and endogenous GLP-1 in the DMH decreases glucose levels

To examine the effect of central GLP-1 on glucose levels, we use intracerebroventricular (ICV) injection of GLP-1R agonist. ICV administration of exendin-4 (Exn4) significantly decreased fasting blood glucose levels (Fig. 1, A and B). c-Fos–positive cell numbers, used as a neuronal activation marker, were increased in the GLP-1R neurons of PVN, ARC (fig. S1, A to C), and DMH (Fig. 1, C and D) after Exn4 administration. The DMH, which receives brainstem GLP-1 projections and expresses GLP-1Rs (*12*, *20*), is a key part of

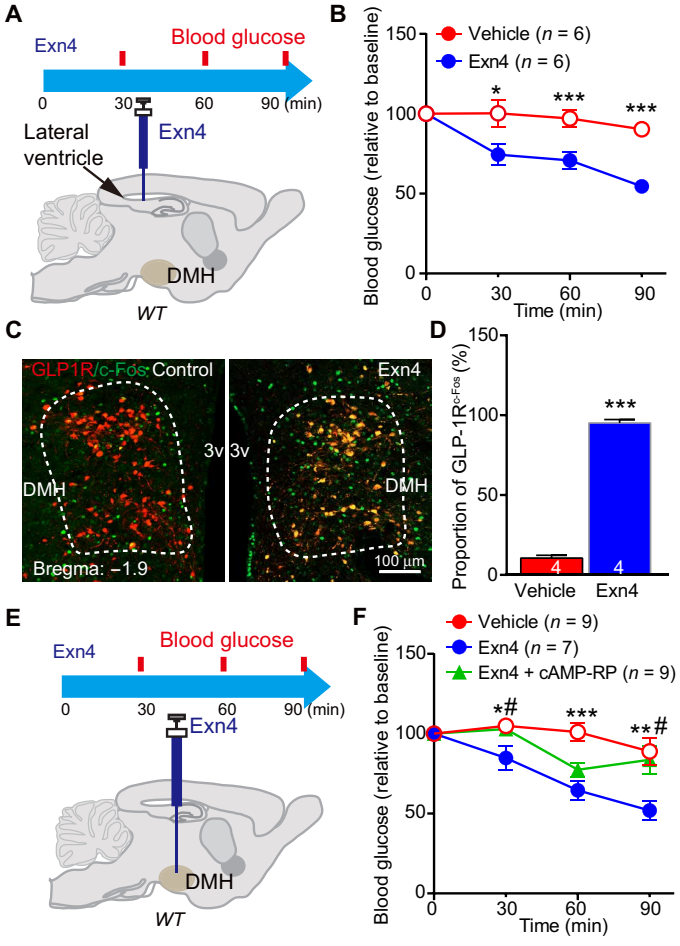

Fig. 1. Exogenous GLP-1 decreases blood glucose level in the DMH. (**A**) Experimental paradigm for ICV injection GLP-1R agonist Exn4 experiment in WT mice. (**B**) ICV Exn4 caused decrease in fasting blood glucose. $^{*}P < 0.05$ and $^{***}P < 0.001$ (*t* test). (**C**) To investigate DMH GLP-1R neuron response to Exn4 injection, we injected adeno-associated virus (AAV)–DIO–mCherry in the DMH of *GLP-1R-Cre* mice and stained with c-Fos antibody. The representative images showed that ICV Exn4 did increase c-Fos expression in GLP-1R neurons within the DMH. (**D**) Quantification of c-Fos–positive cell ration (relative to total GLP-1R neurons). $^{***}P < 0.001$ (*t* test). (**E**) Experimental paradigm for Exn4 injection in DMH of WT mice. (**F**) Fasting blood glucose decreased after Exn4 injection, an effect that was antagonized by the cAMP-PKA blocker, cAMP-Rp. $^{*}P < 0.05$, $^{**}P < 0.01$, and $^{***}P < 0.001$ [analysis of variance (ANOVA)], vehicle versus Exn4; $^{\#}P < 0.05$ (ANOVA), Exn4 versus Exn4 + cAMP-Rp (ANOVA). Numbers of animals are indicated in each panel.

the sympathetic control network (*21*). This suggests that it may play an important role in regulating glucose levels by GLP-1. To test this, we infused Exn4 into DMH through a bilateral guide cannula, which produced a significant reduction of fasting blood glucose levels (Fig. 1, E and F).

Next, we asked whether endogenously released GLP-1 in the DMH has the same function as the exogenously applied GLP-1 agonist. To this end, we used *Gcg-Cre* transgenic mice (*13*, *17*) to selectively target $NTS^{GLP\text{-}1}$-DMH projections and manipulated their activities using both chemogenetic and optogenetic techniques. First, we injected adeno-associated virus (AAV)–mediated selective expression of synaptophysin-mGFP (membrane-targeted green fluorescent protein) into the NTS of *Gcg-Cre* transgenic mice (Fig. 2A and fig. S1E). We found dense clusters of GLP-1 neuronal fibers located in the DMH (Fig. 2B), suggesting that GLP-1–positive neurons send projections to this nucleus. We further confirmed the results by injecting retro-AAV-DIO-GFP into the DMH (injection site shown in fig. S1F) of *Gcg-Cre* transgenic mice (Fig. 2C). We found GFP-labeled GLP-1–positive cells, indicating that those cells were DMH projecting (Fig. 2D). Among those DMH-projecting GLP-1 neurons, more than 80% of them also project to PVN (fig. S2, A and B).

Next, we asked whether $NTS^{GLP\text{-}1}$ neurons form direct synaptic contacts with DMH neurons. Taking advantage of channelrhodopsin 2 (ChR2)–assisted circuit mapping (CRACM) (*22*), we expressed ChR2 in the NTS of *Gcg-Cre* transgenic mice and then performed brain slice recordings in the DMH neurons (Fig. 2E). We detected blue light–evoked excitatory postsynaptic currents (EPSCs) in 7 of 19 DMH neurons from four mice, indicating a possible direct synaptic connection between $NTS^{GLP\text{-}1}$ neurons and DMH neurons (Fig. 2, F and G). AAV-DIO-hM_3Dq-mCherry, a Cre-dependent stimulatory Designer Receptor Exclusively Activated by Designer Drugs (DREADDs), was injected into the NTS of *Gcg-Cre* mice to activate $NTS^{GLP\text{-}1}$ neurons (Fig. 2H and fig. S2C). Administration of the DREADD ligand clozapine *N*-oxide (CNO) by intraperitoneal injection significantly increased c-Fos–positive cell numbers in the DMH (Fig. 2I and fig. S2D), suggesting that DMH neuronal activity can be driven by activation of $NTS^{GLP\text{-}1}$ neurons.

Then, we tested whether targeted activation of $NTS^{GLP\text{-}1}$-to-DMH projections affects blood glucose level by injecting AAV-DIO-ChR2-YFP (yellow fluorescent protein) into the NTS region of *Gcg-Cre* transgenic mice, into which optical fibers had been implanted (bilaterally) in the DMH region (Fig. 2J). Optical stimulation of GLP-1 nerve terminals in the DMH caused a significant reduction of blood glucose in fasting animals (Fig. 2K). This result supports that optogenetic activation of $NTS^{GLP\text{-}1}$-to-DMH projection functions directly in decreasing fasting blood glucose levels. However, it will cause co-releasing GLP-1 and glutamate from activating $NTS^{GLP\text{-}1}$-to-DMH neurons (Fig. 2F). We then investigated whether the endogenously released GLP-1 is required for the control of glucose levels. To do so, we injected retro-AAV-DIO-hM_3Dq into the DMH of *Gcg-Cre* mice to allow expression of excitatory DREADD-hM_3Dq in the DMH-projecting GLP-1 neurons. By local infusion of Exn9 (a specific GLP-1R antagonist) through a guide cannula, we were able to block the GLP-1 signal in the DMH while selectively activating $NTS^{GLP\text{-}1}$-to-DMH projections (Fig. 2L and fig. S2E). Consistent with our optogenetic results (Fig. 2K), stimulation of $NTS^{GLP\text{-}1}$-to-DMH–projecting neurons by CNO alone decreased fasting blood glucose levels, while CNO plus DMH Exn9 treatment completely blocked the hypoglycemic effect (Fig. 2M). To examine whether chemogenetic stimulation of $NTS^{GLP\text{-}1}$ neurons can produce GLP-1 release in the DMH, we collected DMH brain slice and performed enzyme-linked immunosorbent assay (ELISA) after CNO injection and found an increasing trend of DMH GLP-1 concentration when activating $NTS^{GLP\text{-}1}$ neurons chemogenetically (fig. S2F). Together, these findings suggest that endogenous GLP-1 release, induced by stimulation of $NTS^{GLP\text{-}1}$-to-DMH projections, is required for down-regulating blood glucose levels.

$DMH^{GLP\text{-}1R}$ is required for down-regulating blood glucose levels

Given that the presence of GLP in the DMH produced a reduction in blood glucose levels, we next asked whether this down-regulation

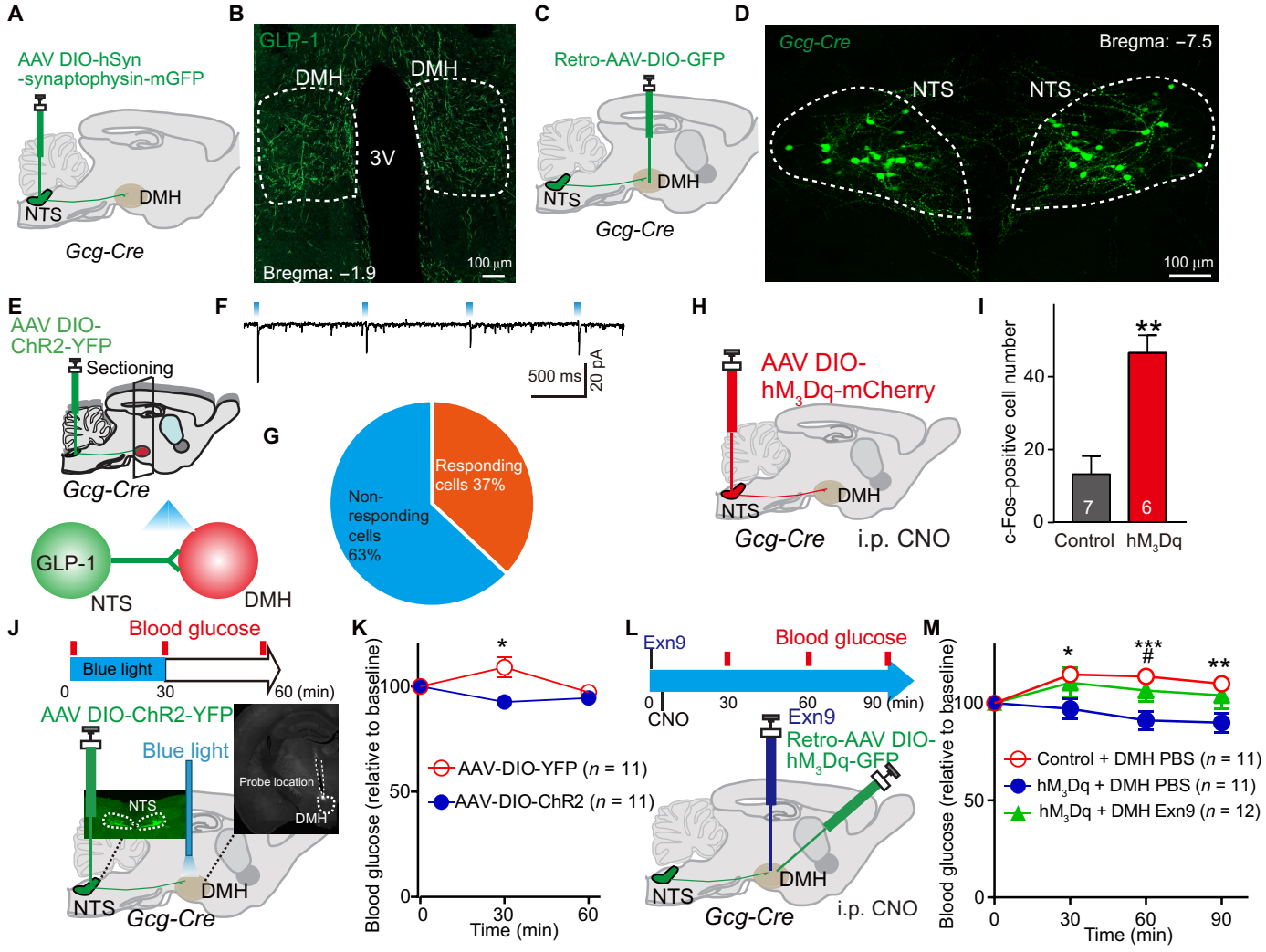

Fig. 2. Endogenous GLP-1 signaling in the DMH decreases blood glucose level. (**A**) Experimental paradigm for synaptophysin-mGFP–mediated synaptic termination tracing in *Gcg-Cre* mice. (**B**) Cre-dependent mGFP expression in the DMH originating from GLP-1 afferents. (**C**) Experimental paradigm for retro-AAV viral injection in *Gcg-Cre* mice. (**D**) Cre-dependent GFP expression in NTS marks GLP-1 neurons *in Gcg-Cre* mice. (**E**) Experimental paradigm for CRACM as we described before (*17*). (**F**) Representative trace of the photostimulation (470-nm light-emitting diode) evoked synaptic currents in DMH neurons in *Gcg-Cre* mice (in 100 μM PTX) (*17*). (**G**) Percentage of neurons showing synaptic connections ($n = 19$ cells from four mice). (**H**) Experimental paradigm for chemogenetic activation of $NTS^{GLP\text{-}1}$ neurons. (**I**) Activation of $NTS^{GLP\text{-}1}$ neurons significantly increased c-Fos expression in the DMH 1 hour after intraperitoneal injection of CNO. $^{**}P < 0.01$ (*t* test). (**J**) Experimental paradigm for optogenetic stimulation of GLP-1 terminals in the DMH. *Gcg-Cre* mice were used: AAV-DIO-YFP (control) and AAV-DIO-ChR2-YFP. Blood was collected at three time points: prestimulation, $t = 0$; during stimulation, $t = 30$; post-stimulation, $t = 60$. (**K**) Fasting blood glucose level is significantly decreased after optogenetic activation of NTS-to-DMH projection. A slight increase on control (YFP) group was observed, which was presumably caused by stress during the experimental process. $^{*}P < 0.05$ (ANOVA test). (**L**) Experimental paradigm for chemogenetic stimulation of $NTS^{GLP\text{-}1}$–DMH. (**M**) Stimulating $NTS^{GLP\text{-}1}$–DMH by intraperitoneal (i.p.) hM_3Dq-specific agonist, CNO significantly decreased fasting blood glucose when compared to control group (retro-AAV-DIO-GFP–infected *Gcg-Cre* mice). Again, a slight increase on vehicle group was observed, which can be induced by the experimental process. $^{*}P < 0.05$, $^{**}P < 0.01$, and $^{***}P < 0.001$ (ANOVA test). Pretreatment with the GLP-1R antagonist Exn9 completely blocked the $NTS^{GLP\text{-}1}$–DMH–induced decreases on fasting blood glucose level. $^{\#}P < 0.05$ (ANOVA test), hM_3Dq + DMH phosphate-buffered saline (PBS) versus hM_3Dq + DMH Exn9. The number of animal used is indicated in each panel. The data presenting style for (E) to (G) and (J) were adapted from our previous publication (*17*).

effect is mediated by GLP-1Rs. To this end, we injected AAV-Cre in the DMH of juvenile *GLP-1R*$^{f/f}$ mice at 5 to 6 weeks of age (Fig. 3A and fig. S3, A and D), which resulted in a ~75% reduction of *GLP-1R* mRNA and protein expression in the DMH (fig. S3, E to I). We observed a moderate but significant gain in body weight (repeated measures, group effect, $P < 0.01$) and epididymal fat (*t* test, $P < 0.01$) when compared to control mice (fig. S3, B and C). This is unlikely induced by food intake because overnight food intake was not different between the control group and *GLP-1R* knockout mice during 7 weeks of observation (repeated measures, group effect, $P = 0.906$; Fig. 3B). Instead, we found a significant decrease in energy expenditure in the GLP-1R ablation group during the dark period (fig. S3J), indicating a possible secondary effect on body weight gain. GLP-1R depletion significantly increased both fasting and refeeding blood glucose levels (repeated measures, $P < 0.05$; Fig. 3, C and D), with the maximal effect observed at around week 4 and then subsiding thereafter (post hoc *t* test, $P < 0.01$ fasting condition and $P < 0.05$ refed condition). To study the impact of the GLP-1 signal on

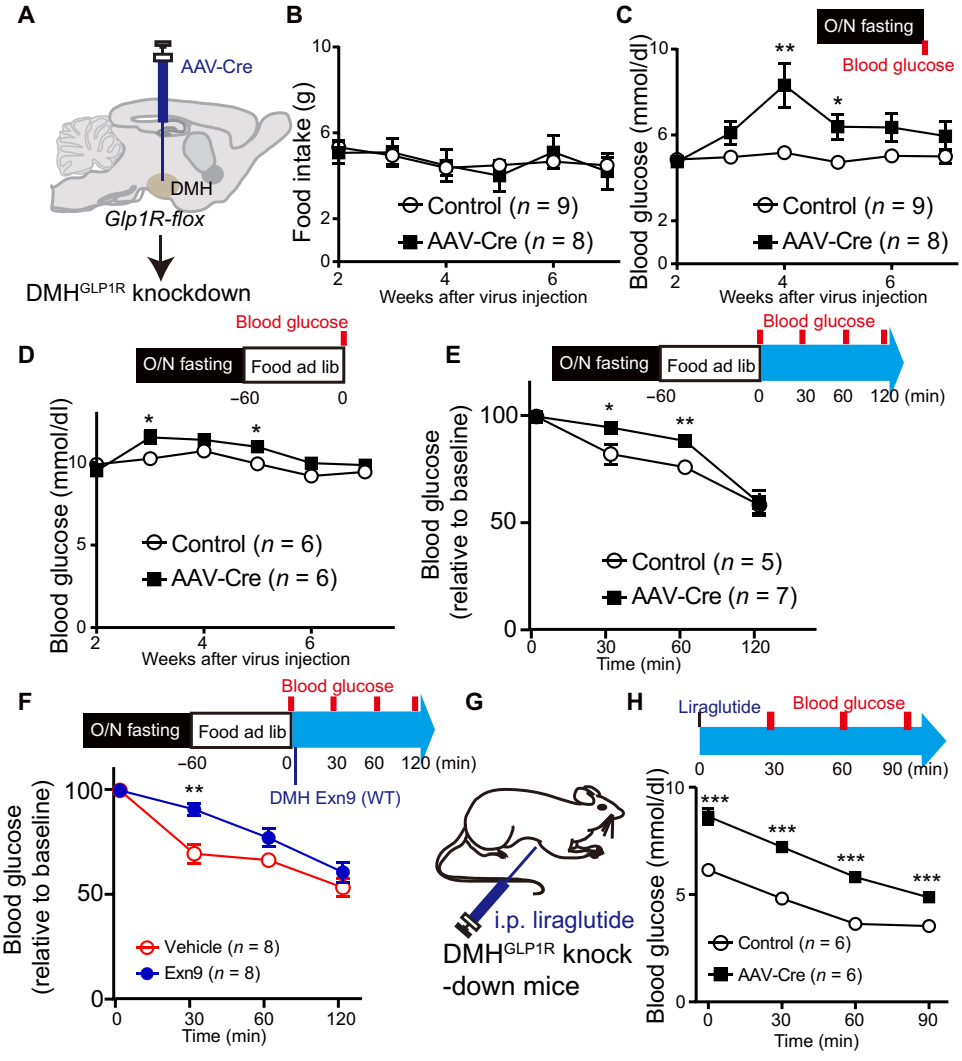

Fig. 3. Ablation of GLP-1R expression in the DMH increases blood glucose level. (**A**) Experimental paradigm for viral injection of AAV-Cre in *GLP1R*$^{f/f}$ mice. (**B**) Overnight food intake is not changed during 7 weeks of observation. (**C**) Fasting blood glucose level increased 4 weeks after GLP-1R depletion from the DMH. **P* < 0.05 and ***P* < 0.01 (repeat measurement with post hoc *t* test). (**D**) To monitor the glucose levels under refed condition, *GLP1R*$^{f/f}$ mice were fasted overnight and then food was available for 1 hour. Blood glucose was measured after 1-hour refeeding and was shown higher in GLP-1R depletion group (repeat measurement: group effect, *P* < 0.05; group × time effect, *P* < 0.05; post hoc ANOVA, **P* < 0.05 at weeks 3 and 5). (**E**) To study the effect of the GLP-1 signal on postprandial glucose, *GLP1R*$^{f/f}$ mice were fasted for overnight. Glucose levels were measured right after 1-hour refeeding, *t* = 0, and then *t* = 30 and 60 min. GLP-1R depletion group showed higher postprandial glucose level when compared to control group (repeat measurement, group effect, *P* < 0.05; post hoc ANOVA, **P* < 0.05, ***P* < 0.01). (**F**) Exn9 was injected into DMH immediately after 1-hour refeeding in WT mice, and the first time point (*t* = 0) for glucose level was measured. Then, glucose levels were measured at *t* = 30 and 60 min. Postprandial glucose significantly increased 0.5 hours after Exn9 injection when compared to vehicle group (repeat measurement, group effect; post hoc ANOVA, *P* < 0.05; ***P* < 0.01). (**G**) Experimental paradigm for GLP-1R agonist liraglutide effect on fasting glucose levels in *GLP1R*$^{f/f}$ mice. (**H**) Fasting blood glucose level decreased in both control and GLP-1R knockdown group after liraglutide injection (repeat measurement, *P* < 0.001, time effect, *P* < 0.001, group effect); post hoc ANOVA analysis showed that blood glucose is higher in GLP-1R knockdown group than in control group, ***P* < 0.01 and ****P* < 0.001. *n* numbers are indicated in each panel.

postprandial glucose, the animals were fasted for 12 hours (overnight). Glucose levels were measured right after 1-hour refeeding, $t = 0$ and then $t = 30$ and 60 min. Food intake within 1 hour was not different between the two groups (fig. S3K). Ablation of GLP-1R in DMH impaired postprandial glucose recovery (repeated measures, $P < 0.05$; Fig. 3E and fig. S3L). Consistently, administration of GLP-1R antagonist Exn9 in the DMH of wild-type (WT) animals caused a higher postprandial glucose level than was seen in the vehicle group (repeated measures, $P < 0.05$; Fig. 3F and fig. S3, M and N), indicating that the DMH GLP-1 signal is required for postprandial glucose recovery. Next, we asked whether GLP-1R inactivation in the DMH affects the glucoregulatory effect of peripheral liraglutide treatment, a GLP-1R agonist. As expected, fasting blood glucose levels decreased after liraglutide injection in both groups ($P < 0.001$, time effect, repeat measurement; Fig. 3, G and H). However, we found a different glucoregulatory effect between the two groups in response to liraglutide treatment ($P < 0.001$, group effect, repeat measurement), and post hoc analysis of variance (ANOVA) analysis showed that blood glucose is higher in the GLP-1R depletion group at $t = 0$, 30, 60, and 90 min ($P < 0.001$; Fig. 3F). Together, these data suggest that

impaired DMH GLP-1R signaling causes dysfunction of glucose homeostasis in adult mice.

GLP-1R activation in DMH antagonizes voltage-gated delayed rectifier potassium current

The above results showed that expression of GLP-1R in the DMH is required for the reduction of blood glucose levels. We next asked whether direct activation of GLP-1R–expressing neurons in the DMH would affect glucose metabolism. The excitatory DREADD hM_3Dq (AAV-DIO-mCherry-hM_3Dq) was expressed in the DMH of *GLP-1R-Cre* mice (Fig. 4A and fig. S4, A to C). We observed a significant decrease in fasting blood glucose level after systemic injection of hM_3Dq-specific agonist CNO (Fig. 4B), indicating that activation of DMH GLP-1R neurons did down-regulate glucose levels.

We showed that the presence of GLP-1 or activation of GLP-1R neurons in DMH could reduce blood glucose levels. However, whether GLP-1 can activate GLP-1R neurons in DMH remains unknown. To address this question, we injected AAV-DIO-mCherry

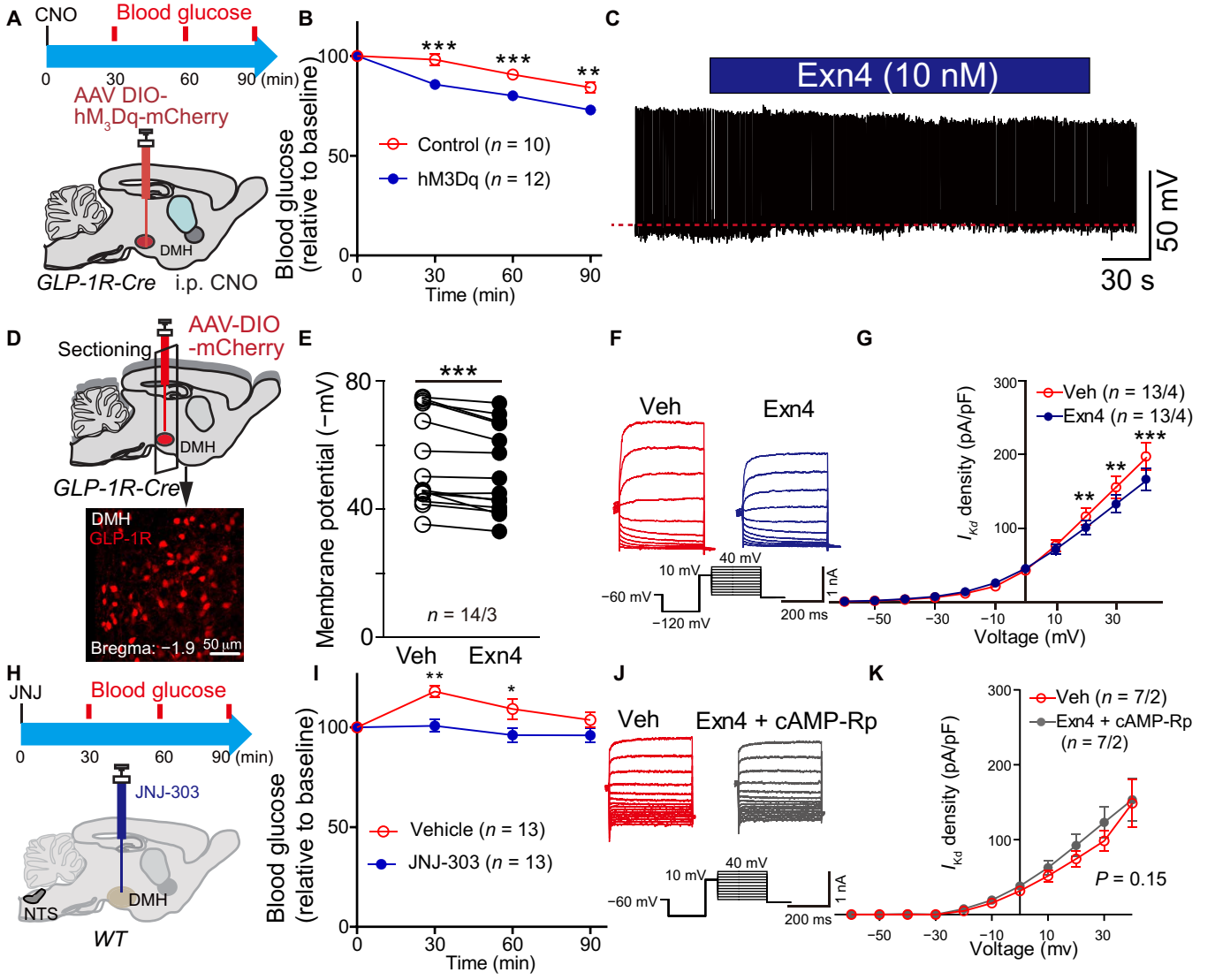

Fig. 4. GLP-1 regulates DMH GLP-1R neuronal activity via suppression of delayed rectifier potassium currents. (**A**) Experimental paradigm for viral injection in *GLP-1R-Cre* mice. (**B**) Activation of GLP-1R neurons in the DMH decreased fasting blood glucose levels after intraperitoneal injection of hM_3Dq-specific agonist, CNO. $^{**}P < 0.01$ and $^{**}P < 0.001$ (ANOVA test), control versus hM_3Dq. (**C**) Representative trace of spontaneous action potential firing after treatment with GLP-1R agonist Exn4 in *GLP-1R-Cre* mice. (**D**) Experimental paradigm for recording GLP-1R–positive neurons within DMH following injection of AAV-DIO-mCherry into *GLP-1R-Cre* mice. (**E**) Membrane potential is significantly increased after Exn4 treatment, indicating depolarization of those cells. $^{***}P < 0.001$ (paired *t* test; $n = 14$ cells from three mice for both groups). (**F**) Representative trace and stimulation protocol for measurement of I_{Kd} before and after Exn4 treatment. (**G**) *I-V* curve shows a right shift after Exn4 treatment, indicating a suppression of I_{Kd}. $^{**}P < 0.01$ and $^{***}P < 0.001$ (repeat measurement and post hoc paired *t* test; $n = 14$ cells from three mice for both groups). (**H**) Experimental paradigm for I_{Kd} blocker JNJ-303 injection in DMH of WT mice. (**I**) Blood glucose decreased after JNJ-303 injection. Again, slight increase on vehicle group was observed, which can be induced by the experimental process. $^{*}P < 0.05$ and $^{**}P < 0.01$ (ANOVA test). (**J**) Representative trace and stimulation protocol for measurement of I_{Kd} before and after Exn4 + cAMP-Rp treatment in *GLP-1R-Cre* mice. (**K**) *I-V* curve shows that Exn4-induced suppression of I_{Kd} can be diminished by blockade of cAMP-PKA signaling (repeat measurement, group effect, $P > 0.05$; group × voltage effect, $P > 0.05$; $n = 7$ cells from two mice for both groups).

to label GLP-1R neurons and characterized spontaneous action potential firing properties with current-clamp recording. Action potential firing rate showed no change with the application of Exn4 (fig. S5, A and B), while membrane potential was significantly depolarized in GLP-1R neurons (Fig. 4, C to E), suggesting that GLP-1 can activate GLP-1R neurons in DMH.

We suspected that GLP-1 could induce GLP-1R neuronal activity by affecting the synaptic transmission or ion channel opening. Application of Exn4 did not change either miniature EPSCs or miniature inhibitory postsynaptic currents (fig. S4, E to J), suggesting that GLP-1 does not affect synaptic transmission in DMH GLP-1R neurons. Analysis of sodium and potassium channel kinetics revealed that the potassium currents were partially blocked by Exn4 (fig. S5, C to F), suggesting that GLP-1 can activate GLP-1R neuronal activity by targeting potassium channels.

Given that the voltage-dependent potassium channel (K_v) currents include the fast A-type potassium current (I_A) and delayed rectifier potassium current (I_{Kd}), we recorded I_{Kd} and I_A using a method that allows for the identification of each current (Fig. 4F and fig. S5G). To subtract I_A, 50 ms of depolarized prepulses (+10 mV) was programmed before voltage steps, and I_A density was subtracted from the trace of I_{Kd}. The plot of mean currents showed that I_{Kd}, but not I_A, was significantly inhibited by application of Exn4 (repeat measurement, voltage × treatment effect, $P < 0.05$ for I_{Kd} and $P = 0.2$ for I_A; Fig. 4G and fig. S5H). Post hoc analysis showed that the current density of I_{Kd} at +20 mV was 116 ± 11 pA/pF in the vehicle control and 101 ± 9 pA/pF with Exn4 treatment ($P = 0.01$); at +30 mV, it was 155 ± 15 pA/pF in control and 133 ± 12 pA/pF with Exn4 treatment ($P < 0.01$); and at +40 mV, it was 196 ± 18 pA/pF in the control and 165 ± 14 pA/pF with Exn4 treatment ($P = 0.001$). Together, activation of DMH GLP-1R partially blocked delayed rectifier K_v channels, but did not rapidly inactivate I_A, resulting in suppression of outward potassium currents and depolarization.

If GLP-1 regulates DMH neuronal activity by suppressing I_{Kd} currents, we would expect a hypoglycemic effect in response blocking K_v channels on GLP-1R neurons. Consistent with this hypothesis, direct infusion of JNJ-303, a specific delayed rectifier K_v blocker, into the DMH recapitulated the Exn4-induced decrease in fasting blood glucose level (Fig. 4, H and I).

Previous studies have indicated that adenosine 3′,5′-monophosphate (cAMP) may regulate I_{Kd} (*23*) and that GLP-1 can activate protein kinase A (PKA) signaling (*24*). Therefore, we next tested whether down-regulation of I_{Kd} in DMH GLP-1R neurons is cAMP-PKA pathway dependent. We used Rp-cAMP (a cAMP-PKA–specific blocker) during I_{Kd} recordings. As expected, the GLP-1R activation–induced inhibition of I_{Kd} current density was completely blocked by Rp-cAMP (repeat measurement, voltage × treatment effect, $P = 0.542$; Fig. 4, J and K), indicating that activation of the cAMP-PKA pathway is required for the effect of GLP-1 on I_{Kd}.

Following the discovery that Rp-cAMP can block the GLP-1–induced inhibition of I_{Kd} current density, we next asked whether Rp-cAMP can block the GLP-1–induced suppression of blood glucose levels. To test this, we infused Rp-cAMP into the DMH before application of Exn4 through a guide cannula. We found that cotreatment with Rp-cAMP blocked Exn4-induced down-regulation of fasting blood glucose level (group effect, vehicle versus Exn4 treatment, $P < 0.01$; vehicle versus Exn4 + Rp-cAMP treatment, $P = 0.752$; Fig. 1F), suggesting that activation of the cAMP-PKA pathway in the DMH is required for GLP-1's effect on blood glucose levels.

Nutritional status regulates the decreasing effect of GLP-1 on blood glucose levels

Although activation of DMH GLP-1R neurons can decrease blood glucose levels in both fasting and refed mice (Figs. 4, A and B, and 5, A and B, and fig. S4D), previous studies indicate that central GLP-1 regulation of feeding behavior is likely dependent on the nutritional status (*8*, *18*). It is still unknown whether DMH GLP-1's effect on glucose metabolism is affected by nutrient states. To address this question, we intraperitoneally injected glucose (2 g/kg body weight) to mimic a high nutrient state in mice. When administrating GLP-1R agonist Exn4 to DMH through a bilateral guide cannula, we found ±52% down-regulation of blood glucose level under high nutrient state (with glucose injection) versus ±19% under low one (without glucose injection) (Fig. 5, C and D). This indicated that Exn4 has a higher ability to decrease blood glucose levels under a high nutrient state than a low one. One of the possible reasons is that Exn4 has a different effect on GLP-1R neuronal activities under different nutrient states.

To understand the GLP-1's effect on GLP-1R neuronal activities under different nutrient states, we use 1 and 5 mM glucose artificial cerebrospinal fluid (ACSF) to mimic the low and high nutrient states, respectively, in vitro. We labeled GLP-1R neurons of the DMH by injecting AAV-DIO-mCherry virus in *GLP-1R-Cre* mice and performed current-clamp recordings following either (i) vehicle perfusion (1 mM glucose, ACSF); (ii) Exn4 + 1 mM glucose, ACSF; or (iii) Exn4 + 5 mM glucose (Fig. 5E). When compared to vehicle, both Exn4 + 1 mM glucose and Exn4 + 5 mM glucose groups showed depolarized membrane potential (Fig. 5, F and G). A significantly increased action potential firing rate was observed in the Exn4 + 5 mM glucose group, but not in the Exn4 + 1 mM glucose group (Fig. 5, F and H). It suggests that GLP-1's stimulating effect on GLP-1R neurons becomes more robust when higher glucose is presented, further supporting a synergistic effect between GLP-1 and glucose.

One possible reason to induce the synergistic effect between GLP-1 and glucose is that DMH GLP-1R neurons are glucose sensing. To this end, we investigated whether 5 mM glucose alone can activate DMH GLP-1R neurons. AAV-DIO-GCaMP6 virus was injected into *GLP-1R-Cre* mice to allow GCaMP6, a calcium signal indicator, expressed in the DMH. Coronal hypothalamic slices (containing DMH) were prepared the same way as an electrophysiological experiment. When switching the perfusion solution from 1 to 5 mM, 20 of 29 cells (from four mice) showed a significant change in $\Delta F/F$. Among the 20 cells, 19 of them showed increased activity during 5 mM glucose perfusion, while one cell showed decreased activity, suggesting that most GLP-1R neurons in the DMH are excited by 5 mM glucose (Fig. 5, I and J). Next, we recorded the neuronal firing activity of GLP-1R neurons in response to 5 mM glucose using whole-cell patch-clamp recording in current-clamp mode. Fifteen of 23 GLP-1R–positive neurons (from four mice) showed at least a 20% change in membrane potential, with 13 cells showing a depolarized potential; two others showed hyperpolarization (Fig. 5, K and L). Together, our experiments have identified a population of glucose-sensing GLP-1R neurons within the DMH.

We also conducted in vivo experiments wherein AAV-DIO-GCaMP6 was injected into DMH of the *GLP-1R-Cre* mice, and an optic fiber was subsequently implanted in the same position to monitor calcium signal changes (fig. S6, A and B). To mimic a high nutrient state, animals were trained to drink mixed glucose (10%)

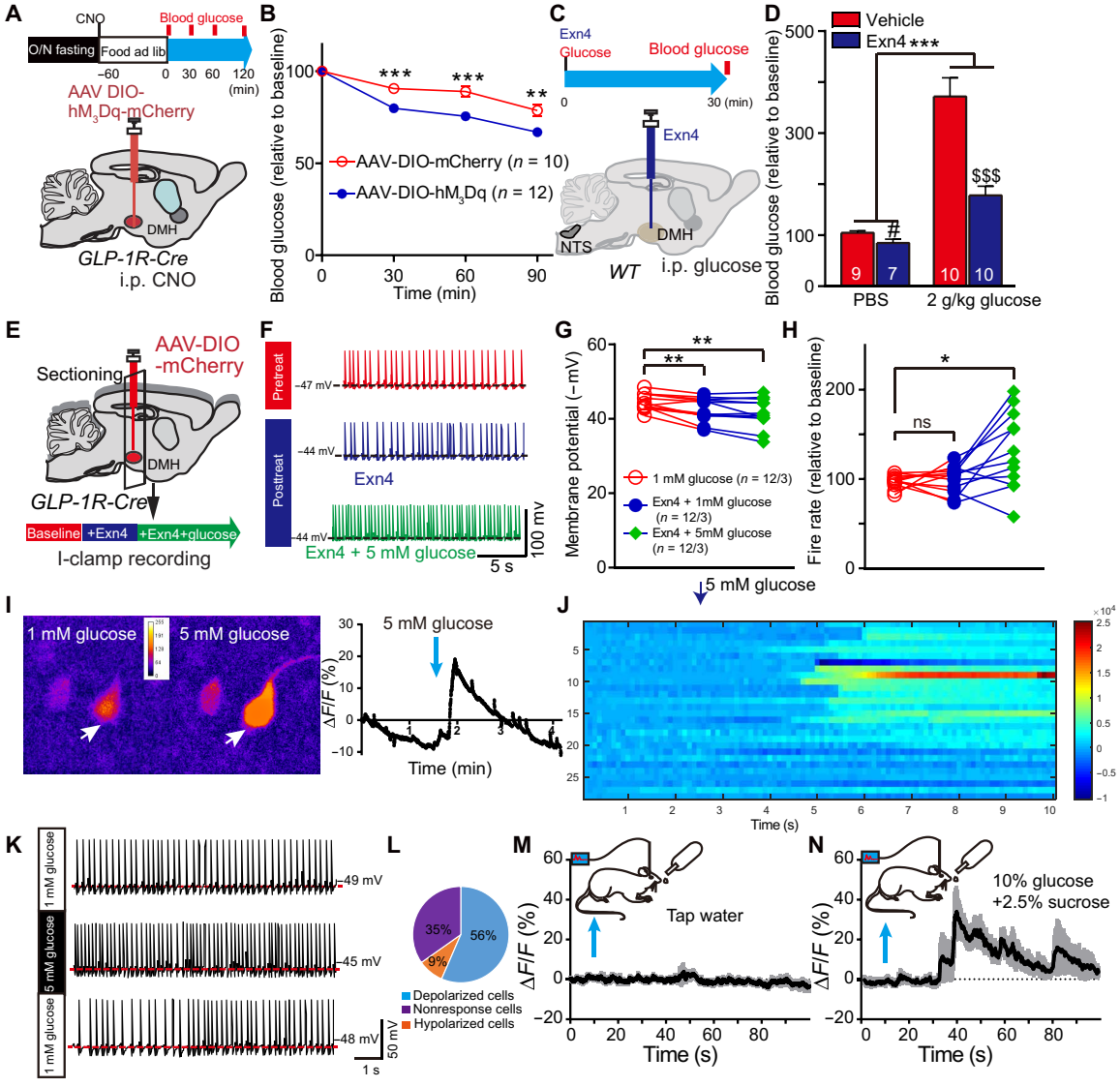

Fig. 5. DMH$^{GLP\text{-}1R}$ neurons are glucose sensing. (**A**) Experimental paradigm for viral injection in *GLP-1R-Cre* mice and time schedule for postprandial glucose measurements. (**B**) Stimulation of DMH GLP-1R neurons significantly decreased blood glucose level when compared to control group in refed condition. $^{**}P < 0.01$ and $^{***}P < 0.001$ (ANOVA test). (**C**) Experimental paradigm for DMH injection with Exn4 and intraperitoneal injection with glucose (2 g/kg) in WT mice. (**D**) Exn4 decreased blood glucose in both PBS group ($^{\#}P < 0.05$, *t* test) and 2 g/kg glucose group ($^{\$\$\$}P < 0.001$, *t* test). DMH Exn4 showed a greater ability to lower blood glucose after intraperitoneal glucose injection. $^{***}P < 0.001$, Exn4 × glucose effect. (**E**) Experimental paradigm for the investigation of Exn4 effects on GLP-1R neuronal activity. (**F**) Representative trace for recording I-clamp from GLP-1R neurons. (**G**) Membrane potential is significantly increased after Exn4 + 1 mM glucose or Exn4 + 5 mM treatment. $^{**}P < 0.01$ (paired *t* test; $n = 12$ cells from three mice). (**H**) Exn4 + 5 mM but not Exn4 + 1 mM treatment significantly increased firing rate of GLP-1R neurons. $^{*}P < 0.05$ (paired *t* test). (**I**) Representative cell responses of DMH GLP-1R neurons to 5 mM glucose treatment (pointed by white arrow). (**J**) Overall, 20 of 29 DMH GLP-1R cells (from four mice) showed a significant change in $\Delta F/F$ during 5 mM glucose perfusion. (**K**) Representative trace for recording I-clamp from GLP-1R neurons during perfusion with 5 mM glucose in *GLP-1R-Cre* mice. (**L**) Thirteen of 23 neurons sampled were shown to be glucose excitable, while two cells are inhibited by 5 mM glucose perfusion. (**M**) No significant change in calcium signal for DMH GLP-1R neurons was found during tap water consumption, while a 30% change in fluorescence was observed during intake of a glucose and sucrose solution ($n = 4$). (**N**) Data in (M) and (N) are presented at mean with SEM in shadow.

and sucrose (2.5%) water solution after overnight food and water deprivation. As expected, blood glucose increased in 5 min of glucose consumption (10% glucose + 2.5% sucrose, ±11.7 mg/dl versus tap water ±6.5 mg/dl; fig. S6, C and D). Concurrently, the Ca^{2+} signal increased (indicated by $\Delta F/F$) by about 30% compared to baseline. No significant changes in bulk Ca^{2+} signals were found when animals consumed tap water (Fig. 5, M and N), suggesting that DMH GLP-1R neurons can sense circulating glucose levels.

Descending control of DMH-DMV-pancreas activity mediates the decreasing effect of GLP-1 on blood glucose levels

Next, we sought to identify downstream targets of DMH$^{GLP\text{-}1R}$ neurons that might mediate glucose-lowering effects. Following injection of AAV-DIO-synaptophysin-GFP into the DMH of *GLP-1R-Cre* mice (Fig. 6A and fig. S6E), dense labeled terminals were found in brainstem regions, including the NTS, dorsal motor nucleus of the vagus nerve (DMV), and raphe pallidus nucleus (RPa), but not in the

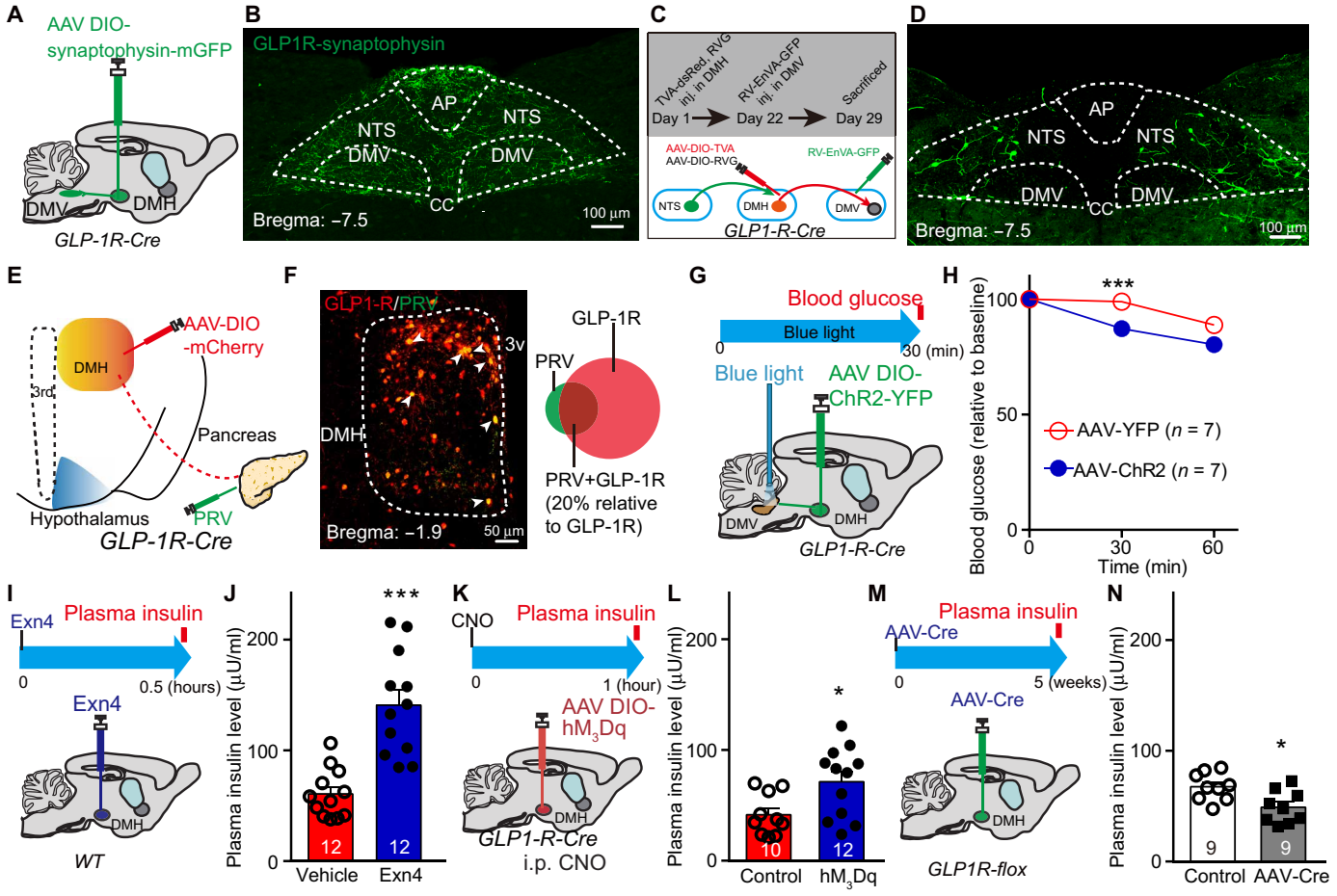

Fig. 6. A descending control of DMH-DMV-pancreas activity mediates the decreased effect of GLP-1 on blood glucose levels. (**A**) Experimental paradigm for synaptophysin-mGFP–mediated anterograde viral tracing in *GLP-1R-Cre* mice. (**B**) Cre-dependent mGFP expression in the brainstem including NTS and DMV originating from GLP-1R afferents. (**C**) Schematic showing tracing of the input-output relationships between $DMH^{GLP\text{-}1R+}$ neurons. Rabies EnVA-ΔG-GFP virus was injected into the DMV. AAV-DIO-RVG and AAV-DIO-TVA-dsRed were coinjected into the DMH of *GLP-1R-Cre* mice. (**D**) Representative images showing a substantial rabies-GFP signal from DMV-projecting $DMH^{GLP\text{-}1R+}$ neurons in the NTS. (**E**) Schematic showing tracing of $DMH^{GLP\text{-}1R+}$ neuron–pancreas projection: PRV-GFP and AAV-DIO-mCherry were injected into pancreas and DMH, respectively, in *GLP-1R-Cre* mice. (**F**) Representative image showing $GLP\text{-}1R^{+}$ neurons (red) and pancreas-projecting neurons (green). Representative pancreas-projecting $GLP\text{-}1R^{+}$ neurons indicated by white arrow (left). PRV-positive cell proportion (relative to total GLP-1R cells) is about 20% (right). (**G**) Experimental paradigm for optogenetic stimulation of GLP-1R terminals in the DMV in *GLP-1R-Cre* mice. $t = 0$, prestimulation, $t = 30$, during stimulation, $t = 60$, post-stimulation. (**H**) Fasting blood glucose level is significantly decreased after exposure to blue light in AAV-DIO-ChR2-YFP–infected *GLP-1R-Cre* mice when compared to the control group (AAV-DIO-YFP–infected *GLP-1R-Cre* mice). $^{***}P < 0.001$ (ANOVA test). (**I**) Experimental paradigm for Exn4 injection in DMH of WT mice. (**J**) Fasting plasma insulin level increased 0.5 hours after Exn4 injection. $^{***}P < 0.001$ (*t* test). (**K**) Experimental paradigm for viral injection in DMH of *GLP-1R-Cre* mice. (**L**) Activation of GLP-1R neurons in the DMH increased fasting plasma insulin levels 1 hour after intraperitoneal injection of hM_3Dq-specific agonist, CNO. $^{*}P < 0.05$ (*t* test). (**M**) Experimental paradigm for viral injection of AAV-Cre in $GLP1R^{f/f}$ mice. (**N**) Plasma insulin levels are significantly lower in GLP-1R knockdown group than in control group. $^{*}P < 0.05$ (*t* test). *n* numbers are indicated in each panel.

intermediolateral nucleus (IML; Fig. 6B and fig. S6, F and G). Although both dorsal vagal complex (DVC) and RPa received afferents from $DMH^{GLP\text{-}1R}$, chemogenetic stimulation of $DMH^{GLP\text{-}1R}$ increased c-Fos expression in the DVC, but not in RPa (fig. S6, H to J). Because DMV plays a critical role in mediating peripheral organ activity, such as liver and pancreas, we further examined these projections using output-specific monosynaptic viral tracing (*25*). *GLP-1R-Cre* mice were infected with AAV-DIO-TVA-dsRed and AAV-DIO-RV-G in the DMH and RV-EnvA-ΔG-GFP in the DMV 4 weeks later (Fig. 6C). Consistent with ChR2-mediated tracing data, frequent GFP^{+} cell bodies were found in the NTS (Fig. 6D), suggesting that an NTS–$DMH^{GLP\text{-}1R}$–DMV circuit can be involved in regulating glucose metabolism.

To answer whether the $DMH^{GLP\text{-}1R}$–DMV circuit regulates glucose levels, we injected AAV-DIO-ChR2-YFP into the DMH region of *GLP-1R-Cre* mice, into which optical fibers had been implanted in the DMV region (Fig. 6G and fig. S6, K and L). Optical stimulation of GLP-1R nerve terminals in the DMV caused a significant reduction of blood glucose in fasting animals (Fig. 6H), indicating that stimulation of the $DMH^{GLP\text{-}1R}$–DMV circuit down-regulates glucose levels.

DMV sends the descending fibers of the vagus nerve to both liver and pancreas branches, which regulates glucose homeostasis and insulin release, respectively (*26*, *27*). To isolate the "brain-periphery" connection between $DMH^{GLP\text{-}1R}$ neurons and peripheral metabolic center, we injected AAV-DIO-mCherry in the DMH of *GLP-1R-Cre*

mice and the trans-synaptic retrograde tracing agent, pseudorabies virus (PRV), into the liver and pancreas, respectively (Fig. 6E and fig. S6M). We found frequent GFP^+ neurons in DMH when injecting PRV-GFP into the pancreas, while few GFP^+ neurons were found when injecting PRV-GFP into the liver (Fig. 6F and fig. S6N), suggesting a DMH-pancreas connection instead of DMH-liver connection. We found colocalization of GFP-labeled pancreas PRV and mCherry-labeled GLP-1R in the DMH, indicating a $DMH^{GLP\text{-}1R}$–pancreas projection (Fig. 6F). Thus, stimulation of DMH GLP-1R may regulate pancreas activity, resulting in insulin level change. To test this, we infused Exn4 into DMH via bilateral guide cannulas and found that plasma insulin levels significantly increased when compared to the vehicle group (Fig. 6, I and J). Consistently, stimulation of $DMH^{GLP\text{-}1R}$ neuronal activity chemogenetically also upregulated plasma insulin levels (Fig. 6, K and L), while inactivating GLP-1R in DMH decreased plasma insulin levels (Fig. 6, M and N). It suggests that DMH GLP-1's effect on glucose levels can be induced by insulin release through the cross-talk between the hypothalamus and pancreas.

DISCUSSION

In the present study, we discovered a population of glucose-sensitive GLP-1R neurons in the DMH, by which endogenous GLP-1 down-regulates glucose level via blockage of delay rectifier potassium channels in a cAMP-PKA–dependent pathway. The input-output organizations revealed that the activation of $DMH^{GLP\text{-}1R}$–induced glucose-lowering effect can be mediated by descending controls of hypothalamus-brainstem-pancreas activity.

Although previous studies suggest that peripheral, rather than central, GLP-1R signaling is essential for the glucose-lowering effect mediated by this receptor (*28*, *29*), acute manipulation of central GLP-1 signaling has also been shown to regulate glucose homeostasis (*14*, *28*, *30*). $NTS^{GLP\text{-}1}$ neurons receive direct synaptic inputs from vagal afferent neurons (*31*, *32*). It has been reported that gastrointestinal distension and large liquid intakes can induce c-Fos expression in this NTS population (*33*, *34*). Recent studies indicated that $NTS^{GLP\text{-}1}$ projecting vagal afferent neurons could be activated by peripheral oxytocin but not GLP-1 (*35*). It is a fundamental question of how the ascending information is sent from $NTS^{GLP\text{-}1}$ to the hypothalamus and processed to control energy metabolism. In a previous study, we discovered an $NTS^{GLP\text{-}1}$–PVN pathway, by which central GLP-1 can regulate feeding behavior (*17*). Here, we presented an $NTS^{GLP\text{-}1}$–DMH pathway down-regulating blood glucose level, suggesting that the DMH GLP-1 signal is able to regulate glucose homeostasis. Both PVN and DMH receive ascending afferents from $NTS^{GLP\text{-}1}$ (fig. S2, A and B). Although PVN-projecting and DMH-projecting GLP-1 neurons are largely overlapped, functions mediated by these two nuclei are different. As the PVN GLP-1 functioned on feeding behavior (*17*, *28*), DMH GLP-1 altered glucose levels and energy metabolism. The different readout can be induced by targeting glucose-sensing GLP-1R neurons in the DMH and the downstream vagal controls.

Sensing of peripheral glucose levels by the hypothalamus plays an important role in maintaining blood glucose levels. Glucose-sensing neurons have been identified in several hypothalamic nuclei: ARC, lateral hypothalamus, paraventricular nucleus, and ventromedial nucleus (*36*–*40*). It has also been reported that glucose-sensing neurons are found in the DMH (*41*). Glucose-sensing neurons are broadly divided into two groups: glucose-excited (GE) and glucose-inhibited (GI). GE neurons show enhanced neuronal activity in response to higher ambient glucose concentrations, while the reverse is true for GI neurons (*36*, *42*–*44*). Our results revealed that most glucose-sensing GLP-1R neurons are the GE type, by which central GLP-1 signaling and peripheral glucose signals are integrated to regulate glucose levels.

GLP-1 regulation of feeding behavior and glucose level is known to be dependent on the nutritional state (*8*, *18*). Here, we used 1 and 5 mM glucose to mimic low and high nutrient states, respectively (*38*, *45*). Although either GLP-1R agonist Exn4 or 5 mM glucose can activate GLP-1R neurons to a certain degree, the activation effect became more robust when both Exn4 and 5 mM glucose were present. This indicates that Exn4 can have a synergistic effect with glucose on the regulation of GLP-1R neuronal activity. Thus, we hypothesize that, as a high nutrient state, the DMH GLP-1 signal affects postprandial glucose recovery. Our *GLP-1R* knockout model and Exn9 antagonist experiments suggest that the DMH GLP-1R signal can be required for postprandial glucose recovery.

Using rigorous viral-mediated neural tracing, we can dissect the connections between central GLP-1R neurons and the peripheral metabolic center, i.e., the pancreas. Our results support that $DMH^{GLP\text{-}1R}$ neurons control pancreas rather than liver activity. Neural-pancreatic research has revealed that, in addition to the pancreatic hormones and peptides, the DVC is a major brain region involved in mediating insulin secretion (*46*, *47*). In our study, the $DMH^{GLP\text{-}1R}$–DMV circuit regulates glucose levels. Thus, we demonstrated a descending control of $DMH^{GLP\text{-}1R}$–DMV–pancreatic activity, mediating the central GLP-1 effect on glucose metabolism (Fig. 7A), although RPa, which mediates a sympathetic activity (*41*, *48*), also receives some afferents from $DMH^{GLP\text{-}1R}$ (fig. S6G). There are only a few $c\text{-}Fos^+$ cells in the RPa when compared to the DVC after stimulating DMH GLP-1R neurons. It suggested that DMH GLP-1R neurons primarily targeted parasympathetic nerve to control pancreas activity. Our results are consistent with previous studies, which indicated that DMH neurons are the second-order parasympathetic pancreas-projecting neurons or could be the third-order sympathetic pancreas-projecting neurons (*49*). In addition, a close interaction between the parasympathetic and sympathetic motor nuclei may also regulate insulin release (*50*, *51*). Further studies are needed to address whether a dual regulatory role is induced by $DMH^{GLP\text{-}1R}$ on both sympathetic and parasympathetic nerve activity.

Although recent studies showed that conditional knockout of GLP-1R in *nestin-Cre* or *Nkx2.1-Cre* mice had no impact on the glucose metabolism (*28*, *29*), we suspect that, in this instance, a developmental compensatory effect can occur during embryogenesis. In the present study, we used strategies involving the injection of AAV-Cre to block GLP-1R expression in adult $GLP\text{-}1R^{f/f}$ mice. As our data demonstrated, impaired GLP-1R expression in the DMH caused an increased blood glucose level without interrupting food intake, which is different from what we observed in PVN (*17*), indicating that a distinct GLP-1 effect can exist between PVN and DMH. There was a glucose surge at around 4 weeks after virus injection, followed by a drop to a relatively lower and stable level, implying that a compensatory mechanism for normalizing glucose levels may develop over time. The increased glucose level is not likely induced by the secondary effect of feeding because overnight feeding is not altered during the 7 weeks of observations. Although we

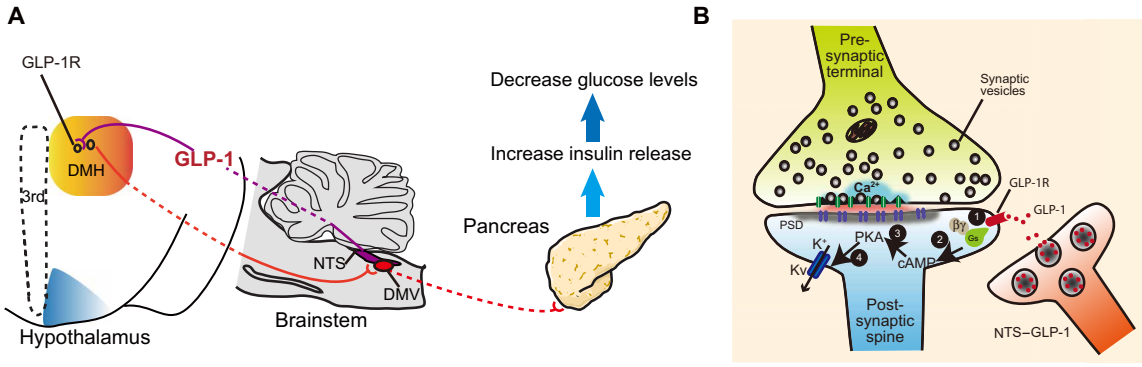

Fig. 7. Cross-talk between central GLP-1 signal and pancreas mediates glucose-lowering effects. (**A**) Descending controls of $NTS^{GLP\text{-}1}$–$DMH^{GLP\text{-}1R}$–DMV–pancreas activity affect glucose level. (**B**) GLP-1 binding to GLP-1R increases intracellular cAMP levels, followed by suppression of voltage-gated potassium currents, inducing a depolarization of the postsynaptic neuron.

found an increase in body weight gain at week 5, the change in glucose levels was earlier (at week 4). Likewise, the body weight gain is likely to be induced by decreased energy expenditure in GLP-1R knockdown mice. Considering that changes in energy expenditure may also affect glucose metabolism and insulin release, we cannot exclude the possible secondary glucoregulatory effect resulting from energy metabolism.

We previously showed that GLP-1R activation in the PVN augments excitatory synaptic strength in PVN neurons, with GLP-1R activation promoting a PKA-dependent signaling cascade leading to phosphorylation of serine-845 on GluA1 AMPA receptors and their trafficking to the plasma membrane (*17*). The present investigation of GLP-1R neuron activation in the DMH detected no such AMPA receptor–mediated downstream signaling events. Instead, our data suggest that GLP-1R activation suppresses delayed rectifier potassium channel–mediated currents, rather than rapidly inactivating potassium currents, which results in the depolarization of the membrane potential. Previous studies showed that the cAMP-PKA pathway could suppress delayed rectifier K_v channels (*5*, *23*, *24*, *52*–*55*); our work suggests that the GLP-1R activation–induced reduction of K_v can also be controlled by cAMP-PKA activity. Thus, our data indicate that the signaling pathway involved in the GLP-1 regulation of DMH neurons can progress as follows: An elevation in intracellular cAMP levels activates PKA signaling, which leads to the blockade of the delayed rectifier potassium channel, resulting in postsynaptic neuronal depolarization and excitation (Fig. 7B).

We want to point out that although we dissected a descending control from central GLP-1 to pancreas activity in this study, we cannot exclude other possible factors that may contribute to the glucoregulatory effect, i.e., the energy expenditure. Moreover, we do not have direct evidence to show that the vagal control insulin release is by targeting β cells of the pancreas islet. Further studies are needed to address those exciting questions.

In summary, our studies highlighted the importance of central GLP-1 signaling in nutrient state–dependent regulation of glucose metabolism by targeting glucose-sensing GLP-1R neurons in the DMH. The input-output organizations revealed that a descending control of DMH-brainstem-pancreas activity could contribute to the glucose-lowering effect.

MATERIALS AND METHODS

Animals

All procedures involving mice were approved by the Institutional Animal Care and Use Committee from Rutgers Robert Wood Johnson Medical School and the University of Science and Technology of China. All animals used in this study were 6- to 8-week-old males unless otherwise stated. The animals are bred in the facility at ~22°C and 35 to 55% humidity. The *Gcg-Cre* transgene was created by insertion of Cre-recombinase into the *Gcg* gene locus of BAC (bacterial artificial chromosome) RP23-242F22 at the ATG start codon as previously described (*13*). *GLP-1R-Cre* mice were purchased from The Jackson Laboratory (strain no. 029283). WT mice C57BL/6 and *GLP-1R-flox* mice were purchased from GemPharmatech (T005818, Nanjing, China). WT mice C57BL/6 were purchased from The Jackson Laboratory. In all cases, mice were randomized according to body weight. The investigator was blinded to the treatment groups except electrophysiological experiments. The sample size required was estimated to be $n = 6$ to 12 per group on the basis of previous studies examining the effects of GLP-1 on feeding behavior (*17*). All procedures had been conducted by at least three biological repeats.

AAV virus

The AAV viruses used in this study include AAV-hSyn-DIO-hM_3Dq-mCherry, retro-AAV-hSyn-DIO-hM_3Dq-mCherry, AAV-hSyn-DIO-mCherry, AAV-EF1a-DIO-ChR2-YFP, retro-AAV-hSyn-DIO-GFP, AAV-hSyn-Cre, and AAV-EF1a-DIO-GFP (purchased from the University of North Carolina Gene Therapy Center). The ChR2-YFP encodes a membrane-bound fusion protein, allowing visualization of both the cell bodies and axons of Cre-expressing neurons for morphologic analyses (*17*). Viral-mediated protein expression was allowed for a period of 14 days before experimental manipulation. Injection sites were confirmed by cutting brain sections and inspecting them under a stereoscope or microscope in all animals reported in this study (*17*). In total, 0.2 μl of virus was used for the injection of the Cre-dependent expression AAV virus, and 60 nl of virus was used for the injection of non-Cre–dependent expression (*17*). The injection speed was 0.1 μl/5 min, while the injection coordinates for NTS were as follows: anteroposterior (AP), −3.4 mm from lambda; lateral (L), ±0.5 mm; ventral (V), 4.125 mm. The injection coordinates for the DMH were as follows: AP, −1.6 mm from bregma; L, ±0.5 mm; V, 5.0 mm.

For PRV-mediated trans-synaptic tracing, 0.1 μl of AAV-DIO-mCherry was injected in DMH of *GLP-1R-Cre* mice. Two weeks later, 0.25 μl of PRV-GFP was injected into the liver or pancreas and then the mice were sacrificed 5 days after PRV injection. Hypothalamic slices were harvested and observed by confocal microscopy (Zeiss, LSM880).

ChR2-assisted circuit mapping

Gcg-Cre animals were injected by AAV-hSyn-DIO-ChR2-YFP into NTS. Two weeks after surgery, mice were deeply anesthetized with Euthasol before sacrifice. Coronal hypothalamic slices (300 μm) were prepared, and whole-cell patch-clamp recordings were performed at 30°C in ACSF containing 125 mM NaCl, 2.5 mM KCl, 1.25 mM NaH_2PO_4, 25 mM $NaHCO_3$, 2.5 mM glucose, 22.5 mM sucrose, 2.5 mM $CaCl_2$, and 1.2 mM $MgCl_2$. Photostimulation-evoked EPSCs were recorded in the whole-cell voltage-clamp mode, with membrane potential clamped at −70 mV (*17*). Photostimulation-evoked EPSCs were recorded in the presence of picrotoxin (100 μM) to block inhibitory postsynaptic currents (*17*). All recordings were made using a multiclamp 700B amplifier, and data were filtered at 2 kHz and digitized at 10 kHz. To photostimulate ChR2-positive fibers, a light-emitting diode (LED) light source was used to generate 470-nm blue light, which was focused on the back aperture of the microscope objective, producing a wide-field exposure of the DMH area (*17*). The photostimulation-evoked EPSC detection protocol was used as described previously (*56*) and involved four blue light laser pulses administered 1 s apart during the first 4 s of an 8-s sweep, repeated for a total of 16 sweeps.

Immunohistochemistry

Mice were deeply anesthetized with Euthasol and transcardially perfused with 4% paraformaldehyde in phosphate-buffered saline (PBS), pH 7.4. Coronal brain slices (35 μm) were prepared, and a standard immunohistochemistry protocol was followed (*17*). The primary antibody used was rabbit anti–c-Fos (1:1000; Abcam, ab-222699 RRID: AB_2891049). Alexa Fluor secondary antibodies (633-goat anti-rabbit; 1:1000; Life Technologies, A21052, RRID: AB_2535719) were used to visualize the signal, and images were acquired by confocal microscopy (Zeiss, LSM880) (*17*).

Depletion of GLP-1R expression in DMH

Each cage of *GLP-1R*$^{f/f}$ mice (four animals) was divided into two groups: Two of them were injected with the AAV-Cre virus into the DMH bilaterally using the following coordinates: AP, −1.6; L, ±0.5; V, 5.0. Another two received an injection of the control virus (AAV-GFP virus). The animals were allowed to recover from surgery for 2 weeks. Body weight, fasting glucose level, and overnight food intake were monitored every week, 2 weeks after surgery. For the refed glucose, the animals were fasted for 12 hours (overnight). The first time point ($t = 0$) for glucose measurement is right after 1-hour refeeding, and then glucose levels were measured at $t = 30$ and 60 min. At week 4, we intraperitoneally injected liraglutide (300 μg/kg; Novo Nordisk) in both the DMH$^{GLP\text{-}1R}$ ablation group and control group. The blood glucose levels were measured at $t = 0$ (before drug injection) and $t = 30$, 60, and 90 min. The animals were sacrificed at week 7; epididymal fat was separated and measured. The brains were cut in precold ACSF by 300 μm thickness, the DMH was separated immediately, mRNA was extracted for quantitative polymerase chain reaction (qPCR) analysis, and protein was saved in -80°C until further analysis. For Western blotting, anti–GLP-1R (ab39072, Abcam, RRID: AB_880213) and horseradish peroxidase anti-rabbit (31460, Life Technologies, RRID: AB_228341) were used for primary and secondary antibody, respectively. For qPCR, the primers used for *GLP-1R* and *GAPDH* gene are as follows: *GLP-1R*, *GGGCCAGTAGTGTGCTACAA* (forward) and *CTTCACACTCCGACAGGTCC* (reverse); *GAPDH*, *GTTTGTGATGGGCGTGAACC* (forward) and *ATGCCGAAGTTGTCGTGGAT* (reverse).

Behavior experiments

Optogenetic manipulation of GLP-1 fibers.

Optical fibers [200 μm diameter core, numerical aperture (NA) 0.37] (Thorlabs) were coupled to a fiber optic rotary joint (Prizmatix) and an LED generator (470 nm for stimulation, Prizmatix UHP-T-470-LA) (*17*). A terminal fiber attached to the rotary joint was coupled to a 1.25–outside diameter (OD) zirconium ferrule and a mating sleeve that allowed the delivery of light directly to the brain (*17*). For in vivo photostimulation experiments, 5-ms pulses and 470-nm blue light were given at 10 pulses per second every 4 s for 1 hour (*17*). For the stimulation experiment, animals were provided only 0.5 g of food overnight. All the mice were trained for 4 days to acclimate to the feeding schedule. To measure the fasting blood glucose, a small drop of tail-tip blood (<5 μl) was placed on the test strip of the blood glucometer (Abbott, FreeStyle Freedom Lite) (*17*).

DREADD experiment

We injected retro-AAV-DIO-hM_3Dq-EGFP (enhanced GFP) into DMH in *Gcg-Cre* transgenic animals to enable DMH-projecting *GCG* neurons to express hM_3Dq and then implanted a bilateral guide cannula onto DMH. After 3 weeks of recovery and virus expression, the mice were trained for an additional 4 days to acclimate to the feeding schedule. The animals were then divided into three groups: (i) control (EGFP) + CNO (intraperitoneal injection, 1 mg/kg) + DMH PBS; (ii) hM_3Dq + CNO (intraperitoneal injection, 1 mg/kg) + DMH PBS; and (iii) hM_3Dq + CNO (intraperitoneal injection, 1 mg/kg) + DMH Exn9 (10 μM, 0.5 μl). Fasting blood glucose was monitored at $t = 0$, 30, 60, and 90 min. For the refed glucose, the animals were fasted for 12 hours (overnight). The first time point ($t = 0$) for glucose measurement is right after 1-hour refeeding, and then glucose levels were measured at $t = 30$ and 60 min.

Cannula infusion

The bilateral guide cannulas (RWD, 62024) were implanted into the DMH and fixed to the skull with three screws and cement. The coordinates used for the DMH were as follows: AP, −1.6; L, ±0.5; V, 4.8. After surgery, mice were housed individually, and 2 weeks were allowed for recovery. The cannula location was checked after sacrificing of animals, and data were collected only from animals with proper placement.

To study how the GLP-1 and cAMP-PKA pathway affected glucose metabolism, we injected either vehicle (200 nl of PBS), Exn4 (0. 1 μg/200 nl; Tocris, 1933), or Exn4 + 0.2 mM cAMP-Rp (200 nl; Tocris, 1337) into the DMH using a guide cannula. Fasting blood glucose was monitored at $t = 0$, 30, 60, 90, and 120 min.

To study the effect of the GLP-1 signal on postprandial glucose, the animals were fasted for 12 hours (overnight). Exn9 (0. 1 μg/200 nl; Tocris, 1933) was injected into DMH immediately after 1-hour refeeding, and the first time point ($t = 0$) for glucose level was measured. Then, glucose levels were measured at $t = 30$ and 60 min.

To block the I_{Kd} pathway in the DMH, 200 nl (2.5 μM) of the I_{Kd} inhibitor JNJ-303 (MedChem Express, HY-16953) was locally injected through the guide cannula into DMH. Fasting blood glucose was monitored at t = 0, 30, 60, 90, and 120 min.

Hormone measurement

For blood glucose measurement, a drop of tail blood was applied by glucometer (FreeStyle Lite system, Abbott Diabetes Care Inc., CA, USA). For insulin measurement, about 150 μl of trunk blood was collected before scarification. The plasma samples were harvested and froze until ELISA by centrifuging the blood samples (with anticoagulant) at 1500 rpm for 15 min (4°C). ELISA was performed following the procedure provided by ELISA kits (EMINS, Thermo Fisher Scientific).

For GLP-1 measurement, we express AAV-DIO-hM_3Dq in the NTS of *Gcg-Cre* mice. After intraperitoneally injecting DREADD agonist CNO, we collected the fresh DMH brain slice (300 μm slice × 2) in lysis buffer and then performed ELISA (CSB-E08118, CUSABIO) according to the provided procedure with kits.

Electrophysiology

Electrophysiology was performed as described previously (*57*) with minor modifications. Briefly, mice were deeply anesthetized with Euthasol before sacrifice. Coronal hypothalamic slices (300 μm) were prepared, and whole-cell patch-clamp recordings were performed at 30°C in ACSF containing 125 mM NaCl, 2.5 mM KCl, 1.25 mM NaH_2PO_4, 25 mM $NaHCO_3$, 2.5 mM glucose, 22.5 mM sucrose, 2.5 mM $CaCl_2$, and 1.2 mM $MgCl_2$. Patch pipettes (3.5 to 6 megohms) were pulled from borosilicate glass. Exn4 (10 nM) was applied to activate GLP-1R. For all the slice electrophysiological recordings, we target the DMH region from bregma −1.4 to bregma −2.0 and collected two coronal slices (300 μm each slice). We randomly targeted GLP-1R cells in the dorsal and ventral part of DMH for recording (as we found that only few GLP-1R–positive cells present in the DMH core region; fig. S4B).

For the voltage-clamp protocol, the internal solution contains 126 mM K-gluconate, 10 mM Hepes, 4 mM KCl, 1.7 mM $MgCl_2$, 4 mM Mg–adenosine triphosphate (ATP), 0.3 mM Na_4–guanosine triphosphate (GTP), and 10 mM phosphocreatine. For the I-clamp protocol, the internal solution contains 126 mM K-gluconate, 4 mM KCl, 10 mM Hepes, 4 mM ATP-Mg, 0.3 mM GTP-Na_2, and 10 mM phosphocreatine. GLP-1R neurons were labeled by the previous injection of AAV-DIO-mCherry into the DMH of *GLP-1R-Cre* mice. Whole-cell patch-clamp recordings were performed using an Axon 700B amplifier. Data were filtered at 2 kHz, digitized at 10 kHz, and collected using Clampex 10.2 (Molecular Devices). To record EPSCs, picrotoxin (50 μM; Sigma-Aldrich) was added to block miniature inhibitory postsynaptic currents mediated by γ-aminobutyric acid type A ($GABA_A$) receptors. Tetrodotoxin (1 μM) was added to block action potentials for mEPSC recording. To block the cAMP-PKA pathway, 50-μm cAMP-Rp was applied to ACSF together with 10 nM Exn4. To block I_{Kd}, 250 nM JNJ-303 was applied to ACSF together with 10 nM Exn4.

For recording brain slices under different energy states, mice were fasted overnight (12 hours). Fresh brain slices were made and recovered in low-glucose (1 mM) ACSF solution. During I-clamp recording, 1 mM glucose ACSF was perfused for 5 min to record baseline action potential, followed by another 5 min of 10 nM Exn4 + 1 mM glucose ACSF perfusion, and then 10 nM Exn4 + 5 mM glucose perfusion.

For testing glucose-sensing neurons, mice were fasted overnight (12 hours). The same procedure was used as described above to collect brain slices. During I-clamp recording, 1 mM glucose ACSF was perfused for 5 min to record baseline action potentials, followed by 5 mM glucose perfusion.

Ca^{2+} image and fiber photometry

AAV-hSyn-DIO-Gcamp6 (200 nl) was unilaterally injected in DMH of *GLP-1R-Cre* mice and allowed to express for 3 weeks. The animals were fasted for 12 hours before the experiment.

For in vitro experiments, animals were sacrificed in the morning, and fresh DMH brain slices were made as described in the electrophysiology section. Ca^{2+} images were collected at low-glucose condition (1 mM) and high-glucose condition (5 mM), respectively, by 10 frames/s at a resolution of 1024 μm × 1024 μm (Hamamatsu, C11440). The data were summarized by ImageJ and MATLAB software.

For in vivo experiments, optical fibers (250 μm diameter core, NA 0.37) (Newdoon) were placed on DMH and connected to a fiber photometry setup (ThinkerTech, Nanjing, China). The emission light was generated by a 480-nm LED, reflected with a dichroic mirror, and delivered to the brain to excite the GCaMP6. The emission light was passed through another band-pass filter, into a CMOS (complementary metal-oxide semiconductor) detector (Thorlabs Inc.; DCC3240M), and finally recorded by a LabVIEW program (TDMSViewer, ThinkerTech, Nanjing, China). The animals were trained for 4 days to acclimate to the experiment schedule: (i) water and food deprivation (12 hours), (ii) 30-min baseline recording, and (iii) place water bottle containing either vehicle (tap water) or glucose (tap water + 10% glucose + 2.5% sucrose).

Fiber photometry signals were processed with a custom-written MATLAB software, which is available at https://zenodo.org/record/6456623#.YlaF_8hByUk (Zenodo ID: 6456623; Zenodo DOI: 10.5281/zenodo.6456623; ThinkerTech Nanjing Bioscience, 2020). Briefly, all the data were segmented on the basis of the behavioral events and baseline phase. The change in fluorescence ($\Delta F/F$) was calculated as $(F - F_0)/F_0$, where F_0 represents the baseline fluorescence signal averaged over a 10-s-long control time window.

Quantification and statistical analysis

Statistical analysis was performed using SPSS (version 18) or Excel (version 2013). We first determined whether the data values came from a normal distribution by Kolmogorov-Smirnov test. Repeated-measures two-way ANOVA and post hoc Bonferroni tests were used for all time-dependent experiments (*17*). The cumulative frequency curve was analyzed by the Kolmogorov-Smirnov test (*17*). Outliers are removed by using "Descriptive Statistics" of SPSS. Statistical significance was set at $P < 0.05$. All the details of the experiments can be found in the figure legends. All data values are presented as means ± SEM.

SUPPLEMENTARY MATERIALS

Supplementary material for this article is available at https://science.org/doi/10.1126/sciadv.abn5345

View/request a protocol for this paper from *Bio-protocol*.

REFERENCES AND NOTES

1. G. I. Bell, R. Sanchez-Pescador, P. J. Laybourn, R. C. Najarian, Exon duplication and divergence in the human preproglucagon gene. *Nature* **304**, 368–371 (1983).
2. D. J. Drucker, Glucagon and the glucagon-like peptides. *Pancreas* **5**, 484–488 (1990).

3. D. J. Drucker, Mechanisms of action and therapeutic application of glucagon-like peptide-1. *Cell Metab.* **27**, 740–756 (2018).
4. D. J. Drucker, J. F. Habener, J. J. Holst, Discovery, characterization, and clinical development of the glucagon-like peptides. *J. Clin. Invest.* **127**, 4217–4227 (2017).
5. T. D. Müller, B. Finan, S. R. Bloom, D. D'Alessio, D. J. Drucker, P. R. Flatt, A. Fritsche, F. Gribble, H. J. Grill, J. F. Habener, J. J. Holst, W. Langhans, J. J. Meier, M. A. Nauck, D. Perez-Tilve, A. Pocai, F. Reimann, D. A. Sandoval, T. W. Schwartz, R. J. Seeley, K. Stemmer, M. Tang-Christensen, S. C. Woods, R. D. Di Marchi, M. H. Tschöp, Glucagon-like peptide 1 (GLP-1). *Mol. Metab.* **30**, 72–130 (2019).
6. J. J. Meier, B. Gallwitz, W. E. Schmidt, M. A. Nauck, Glucagon-like peptide 1 as a regulator of food intake and body weight: Therapeutic perspectives. *Eur. J. Pharmacol.* **440**, 269–279 (2002).
7. G. C. Weir, S. Mojsov, G. K. Hendrick, J. F. Habener, Glucagonlike peptide I (7-37) actions on endocrine pancreas. *Diabetes* **38**, 338 (1989).
8. D. Sandoval, J. G. Barrera, M. A. Stefater, S. Sisley, S. C. Woods, D. D. D'Alessio, R. J. Seeley, The anorectic effect of GLP-1 in rats is nutrient dependent. *PLOS ONE* **7**, e51870 (2012).
9. L. A. Scrocchi, B. A. Marshall, S. M. Cook, P. L. Brubaker, D. J. Drucker, Identification of glucagon-like peptide 1 (GLP-1) actions essential for glucose homeostasis in mice with disruption of GLP-1 receptor signaling. *Diabetes* **47**, 632–639 (1998).
10. J. J. Holst, The physiology of glucagon-like peptide 1. *Physiol. Rev.* **87**, 1409–1439 (2007).
11. P. J. Larsen, M. Tang-Christensen, J. J. Holst, C. Orskov, Distribution of glucagon-like peptide-1 and other preproglucagon-derived peptides in the rat hypothalamus and brainstem. *Neuroscience* **77**, 257–270 (1997).
12. G. Gu, B. Roland, K. Tomaselli, C. S. Dolman, C. Lowe, J. S. Heilig, Glucagon-like peptide-1 in the rat brain: Distribution of expression and functional implication. *J. Comp. Neurol.* **521**, 2235–2261 (2013).
13. R. P. Gaykema, B. A. Newmyer, M. Ottolini, V. Raje, D. M. Warthen, P. S. Lambeth, M. Niccum, T. Yao, Y. Huang, I. G. Schulman, T. E. Harris, M. K. Patel, K. W. Williams, M. M. Scott, Activation of murine pre-proglucagon-producing neurons reduces food intake and body weight. *J. Clin. Invest.* **127**, 1031–1045 (2017).
14. D. A. Sandoval, D. Bagnol, S. C. Woods, D. A. D'Alessio, R. J. Seeley, Arcuate glucagon-like peptide 1 receptors regulate glucose homeostasis but not food intake. *Diabetes* **57**, 2046–2054 (2008).
15. D. Perez-Tilve, L. González-Matías, B. A. Aulinger, M. Alvarez-Crespo, M. Gil-Lozano, E. Alvarez, A. M. Andrade-Olivie, M. H. Tschöp, D. A. D'Alessio, F. Mallo, Exendin-4 increases blood glucose levels acutely in rats by activation of the sympathetic nervous system. *Am. J. Physiol. Endocrinol. Metab.* **298**, E1088–E1096 (2010).
16. C. Pyke, R. S. Heller, R. K. Kirk, C. Ørskov, S. Reedtz-Runge, P. Kaastrup, A. Hvelplund, L. Bardram, D. Calatayud, L. B. Knudsen, GLP-1 receptor localization in monkey and human tissue: Novel distribution revealed with extensively validated monoclonal antibody. *Endocrinology* **155**, 1280–1290 (2014).
17. J. Liu, K. Conde, P. Zhang, V. Lilascharoen, Z. Xu, B. K. Lim, R. J. Seeley, J. J. Zhu, M. M. Scott, Z. P. Pang, Enhanced AMPA receptor trafficking mediates the anorexigenic effect of endogenous glucagon-like peptide-1 in the paraventricular hypothalamus. *Neuron* **96**, 897–909.e5 (2017).
18. D. L. Williams, D. G. Baskin, M. W. Schwartz, Leptin regulation of the anorexic response to glucagon-like peptide-1 receptor stimulation. *Diabetes* **55**, 3387–3393 (2006).
19. C. Li, J. Navarrete, J. Liang-Guallpa, C. Lu, S. C. Funderburk, R. B. Chang, S. D. Liberles, D. P. Olson, M. J. Krashes, Defined paraventricular hypothalamic populations exhibit differential responses to food contingent on caloric state. *Cell Metab.* **29**, 681–694.e5 (2019).
20. S. C. Cork, J. E. Richards, M. K. Holt, F. M. Gribble, F. Reimann, S. Trapp, Distribution and characterisation of glucagon-like peptide-1 receptor expressing cells in the mouse brain. *Mol. Metab.* **4**, 718–731 (2015).
21. S. F. Morrison, C. J. Madden, D. Tupone, Central control of brown adipose tissue thermogenesis. *Front. Endocrinol. (Lausanne)* **3**, 5 (2012).
22. L. Petreanu, D. Huber, A. Sobczyk, K. Svoboda, Channelrhodopsin-2-assisted circuit mapping of long-range callosal projections. *Nat. Neurosci.* **10**, 663–668 (2007).
23. M. Aflaki, X.-Y. Qi, L. Xiao, B. Ordog, A. Tadevosyan, X. Luo, A. Maguy, Y. Shi, J.-C. Tardif, S. Nattel, Exchange protein directly activated by cAMP mediates slow delayed-rectifier current remodeling by sustained β-adrenergic activation in guinea pig hearts. *Circ. Res.* **114**, 993–1003 (2014).
24. Y. A. Mei, D. Vaudry, M. Basille, H. Castel, A. Fournier, H. Vaudry, B. J. Gonzalez, PACAP inhibits delayed rectifier potassium current via a cAMP/PKA transduction pathway: Evidence for the involvement of IK in the anti-apoptotic action of PACAP. *Eur. J. Neurosci.* **19**, 1446–1458 (2004).
25. M. R. Gielow, L. Zaborszky, The input-output relationship of the cholinergic basal forebrain. *Cell Rep.* **18**, 1817–1830 (2017).
26. K. N. Browning, F. H. Coleman, R. A. Travagli, Characterization of pancreas-projecting rat dorsal motor nucleus of vagus neurons. *Am. J. Physiol. Gastrointest. Liver Physiol.* **288**, G950–G955 (2005).
27. A. Pocai, S. Obici, G. J. Schwartz, L. Rossetti, A brain-liver circuit regulates glucose homeostasis. *Cell Metab.* **1**, 53–61 (2005).
28. M. A. Burmeister, J. E. Ayala, H. Smouse, A. Landivar-Rocha, J. D. Brown, D. J. Drucker, D. A. Stoffers, D. A. Sandoval, R. J. Seeley, J. E. Ayala, The hypothalamic glucagon-like peptide 1 receptor is sufficient but not necessary for the regulation of energy balance and glucose homeostasis in mice. *Diabetes* **66**, 372–384 (2017).
29. S. Sisley, R. Gutierrez-Aguilar, M. Scott, D. A. D'Alessio, D. A. Sandoval, R. J. Seeley, Neuronal GLP1R mediates liraglutide's anorectic but not glucose-lowering effect. *J. Clin. Invest.* **124**, 2456–2463 (2014).
30. M. A. Burmeister, T. Ferre, J. E. Ayala, E. M. King, R. M. Holt, Acute activation of central GLP-1 receptors enhances hepatic insulin action and insulin secretion in high-fat-fed, insulin resistant mice. *Am. J. Physiol. Endocrinol. Metab.* **302**, E334–E343 (2012).
31. K. Hisadome, F. Reimann, F. M. Gribble, S. Trapp, Leptin directly depolarizes preproglucagon neurons in the nucleus tractus solitarius: Electrical properties of glucagon-like peptide 1 neurons. *Diabetes* **59**, 1890–1898 (2010).
32. M. K. Holt, L. E. Pomeranz, K. T. Beier, F. Reimann, F. M. Gribble, L. Rinaman, Synaptic inputs to the mouse dorsal vagal complex and its resident preproglucagon neurons. *J. Neurosci.* **39**, 9767–9781 (2019).
33. A. D. Kreisler, L. Rinaman, Hindbrain glucagon-like peptide-1 neurons track intake volume and contribute to injection stress-induced hypophagia in meal-entrained rats. *Am. J. Physiol. Regul. Integr. Comp. Physiol.* **310**, R906–R916 (2016).
34. N. Vrang, C. B. Phifer, M. M. Corkern, H. R. Berthoud, Gastric distension induces c-Fos in medullary GLP-1/2-containing neurons. *Am. J. Physiol. Regul. Integr. Comp. Physiol.* **285**, R470–R478 (2003).
35. D. I. Brierley, M. K. Holt, A. Singh, A. de Araujo, M. McDougle, M. Vergara, M. H. Afaghani, S. J. Lee, K. Scott, C. Maske, W. Langhans, E. Krause, A. de Kloet, F. M. Gribble, F. Reimann, L. Rinaman, G. de Lartigue, S. Trapp, Central and peripheral GLP-1 systems independently suppress eating. *Nat. Metab.* **3**, 258–273 (2021).
36. V. H. Routh, L. Hao, A. M. Santiago, Z. Sheng, C. Zhou, Hypothalamic glucose sensing: Making ends meet. *Front. Syst. Neurosci.* **8**, 236 (2014).
37. X. Fioramonti, S. Contié, Z. Song, V. H. Routh, A. Lorsignol, L. Pénicaud, Characterization of glucosensing neuron subpopulations in the arcuate nucleus: Integration in neuropeptide Y and pro-opio melanocortin networks? *Diabetes* **56**, 1219–1227 (2007).
38. Y. He, P. Xu, C. Wang, Y. Xia, M. Yu, Y. Yang, K. Yu, X. Cai, N. Qu, K. Saito, J. Wang, I. Hyseni, M. Robertson, B. Piyarathna, M. Gao, S. A. Khan, F. Liu, R. Chen, C. Coarfa, Z. Zhao, Q. Tong, Z. Sun, Y. Xu, Estrogen receptor-α expressing neurons in the ventrolateral VMH regulate glucose balance. *Nat. Commun.* **11**, 2165 (2020).
39. V. H. Routh, Glucose sensing neurons in the ventromedial hypothalamus. *Sensors (Basel)* **10**, 9002–9025 (2010).
40. A. K. Sutton, P. B. Goforth, I. E. Gonzalez, J. Dell'Orco, H. Pei, M. G. Myers Jr., D. P. Olson, Melanocortin 3 receptor-expressing neurons in the ventromedial hypothalamus promote glucose disposal. *Proc. Natl. Acad. Sci. U.S.A.* **118**, e2103090118 (2021).
41. A. Picard, S. Metref, D. Tarussio, W. Dolci, X. Berney, S. Croizier, G. Labouebe, B. Thorens, Fgf15 neurons of the dorsomedial hypothalamus control glucagon secretion and hepatic gluconeogenesis. *Diabetes* **70**, 1443–1457 (2021).
42. L. Kang, V. H. Routh, E. V. Kuzhikandathil, L. D. Gaspers, B. E. Levin, Physiological and molecular characteristics of rat hypothalamic ventromedial nucleus glucosensing neurons. *Diabetes* **53**, 549–559 (2004).
43. B. E. Levin, A. A. Dunn-Meynell, V. H. Routh, Brain glucosensing and the K(ATP) channel. *Nat. Neurosci.* **4**, 459–460 (2001).
44. Z. Song, B. E. Levin, J. J. McArdle, N. Bakhos, V. H. Routh, Convergence of pre- and postsynaptic influences on glucosensing neurons in the ventromedial hypothalamic nucleus. *Diabetes* **50**, 2673–2681 (2001).
45. J. J. Liu, N. T. Bello, Z. P. Pang, Presynaptic regulation of leptin in a defined lateral hypothalamus-ventral tegmental area neurocircuitry depends on energy state. *J. Neurosci.* **37**, 11854–11866 (2017).
46. K. N. Browning, F. H. Coleman, R. A. Travagli, Effects of pancreatic polypeptide on pancreas-projecting rat dorsal motor nucleus of the vagus neurons. *Am. J. Physiol. Gastrointest. Liver Physiol.* **289**, G209–G219 (2005).
47. E. Ionescu, F. Rohner-Jeanrenaud, H. R. Berthoud, B. Jeanrenaud, Increases in plasma insulin levels in response to electrical stimulation of the dorsal motor nucleus of the vagus nerve. *Endocrinology* **112**, 904–910 (1983).
48. S. J. Lee, G. Sanchez-Watts, J.-P. Krieger, A. Pignalosa, P. N. Norell, A. Cortella, K. G. Pettersen, D. Vrdoljak, M. R. Hayes, S. E. Kanoski, W. Langhans, A. G. Watts, Loss of dorsomedial hypothalamic GLP-1 signaling reduces BAT thermogenesis and increases adiposity. *Mol. Metab.* **11**, 33–46 (2018).

49. R. M. Buijs, S. J. Chun, A. Niijima, H. J. Romijn, K. Nagai, Parasympathetic and sympathetic control of the pancreas: A role for the suprachiasmatic nucleus and other hypothalamic centers that are involved in the regulation of food intake. *J. Comp. Neurol.* **431**, 405–423 (2001).
50. B. Ahren, G. J. Taborsky Jr., The mechanism of vagal nerve stimulation of glucagon and insulin secretion in the dog. *Endocrinology* **118**, 1551–1557 (1986).
51. T. Kurose, K. Tsuda, H. Ishida, K. Tsuji, Y. Okamoto, Y. Tsuura, S. Kato, M. Usami, H. Imura, Y. Seino, Glucagon, insulin and somatostatin secretion in response to sympathetic neural activation in streptozotocin-induced diabetic rats. A study with the isolated perfused rat pancreas in vitro. *Diabetologia* **35**, 1035–1041 (1992).
52. Y. L. He, X. Q. Zhan, G. Yang, J. Sun, Y. A. Mei, Amoxapine inhibits the delayed rectifier outward K+ current in mouse cortical neurons via cAMP/protein kinase A pathways. *J. Pharmacol. Exp. Ther.* **332**, 437–445 (2010).
53. G. Yang, M. H. Zhou, Z. Ren, J. J. Xu, Y.-A. Mei, Amoxapine inhibits delayed outward rectifier K^+ currents in cerebellar granule cells via dopamine receptor and protein kinase A activation. *Cell. Physiol. Biochem.* **28**, 163–174 (2011).
54. Y. Zhang, Y. Zhang, Z. Wang, Y. Sun, X. Jiang, M. Xue, Y. Yu, J. Tao, Suppression of delayed rectifier K^+ channels by gentamicin induces membrane hyperexcitability through JNK and PKA signaling pathways in vestibular ganglion neurons. *Biomed. Pharmacother.* **135**, 111185 (2021).
55. P. E. MacDonald, X. Wang, F. Xia, W. el-kholy, E. D. Targonsky, R. G. Tsushima, M. B. Wheeler, Antagonism of rat beta-cell voltage-dependent K+ currents by exendin 4 requires dual activation of the cAMP/protein kinase A and phosphatidylinositol 3-kinase signaling pathways. *J. Biol. Chem.* **278**, 52446–52453 (2003).
56. M. J. Krashes, B. P. Shah, J. C. Madara, D. P. Olson, D. E. Strochlic, A. S. Garfield, L. Vong, H. Pei, M. Watabe-Uchida, N. Uchida, S. D. Liberles, B. B. Lowell, An excitatory paraventricular nucleus to AgRP neuron circuit that drives hunger. *Nature* **507**, 238–242 (2014).
57. Z. P. Pang, P. Deng, Y. W. Ruan, Z. C. Xu, Depression of fast excitatory synaptic transmission in large aspiny neurons of the neostriatum after transient forebrain ischemia. *J. Neurosci.* **22**, 10948–10957 (2002).

Acknowledgments

Funding: This work was supported by the National Natural Science Foundation of China (91957112 to J.L.), National Natural Science Foundation of China (31970950 to J.L.), Robert Wood Johnson Foundation (no. 74260 to Z.P.P.), National Institutes of Health (grant R01MH116694 to M.M.S.), National Natural Science Foundation of China (nos. 31822026 and 32100821 to C.Z.), and National Key R&D Program of China (2021ZD0203900 to C.Z.). We thank the Institute of Advanced Technology-Huami Joint Laboratory for Brain-Machine Intelligence at the University of Science and Technology of China for partial support (to J.L.). **Author contributions:** Conceptualization: J.L. and Z.P.P. Methodology: L.Y. and Z.X. Investigation: Z.H., L.L., J.N.Z., K.C., and J.P. Visualization: Z.L. and W.W. Supervision: J.L., Z.P.P., and C.Z. Writing—original draft: J.L. and Z.P.P. Writing—review and editing: J.L., Z.P.P., C.Z., F.W., G.B., J.Z., R.J.S., and M.M.S. **Competing interests:** R.J.S. serves as a consultant or scientific advisory board member from Novo Nordisk, Sohia, Kintai Therapeutics, Ionis, Eli Lilly, Zafgen, Calibrate, Rewind, Novo Nordisk, AstraZeneca, Pfizer, and Energesis. The authors declare no other competing interests. **Data and materials availability:** All data needed to evaluate the conclusions in the paper are present in the paper and/or the Supplementary Materials. The MATLAB-based software for fiber photometry signal processing is available at https://zenodo.org/record/6456623#.YlaF_8hByUk (Zenodo ID: 6456623; Zenodo DOI: 10.5281/zenodo.6456623).

Submitted 8 December 2021
Accepted 21 April 2022
Published 8 June 2022
10.1126/sciadv.abn5345